Longitudinal critical angle singularities and their effect on V(Z) of the line-focus-beam acoustic microscope

doi: 10.1109/58.294105

Longitudinal Critical Angle Singularities and their Effect on $V(Z)$ of the Line-Focus-Beam Acoustic Microscope

Yusuke Tsukahara, *Member, IEEE*, Yongshen Liu, Christian Néron, C. K. Jen, *Senior Member, IEEE*, and Jun-ichi Kushibiki, *Member, IEEE*

Abstract—**In order to investigate a mechanism which causes a velocity difference between the longitudinal wave and leaky surface skimming compressional wave (LSSCW) observed in a line-focus-beam acoustic microscope, the analytic property of an acoustic reflection coefficient and its effect on a $V(z)$ analysis were studied. A pole hidden in the unphysical Riemann sheet close to the longitudinal branch point is found to be responsible for the abrupt phase change at the longitudinal critical angle. This, together with an effect of a dominant Rayleigh wave pole, affects the $V(z)$ measurement of the LSSCW. A method to estimate the longitudinal and shear wave velocities is discussed.**

I. Introduction

THE $V(z)$ METHOD in reflection acoustic microscopy offers a useful tool for the analysis of elastic properties of solid materials. Oscillations in the electrical output from an acoustical lens as it moves toward a solid surface were first reported by Weglein [1] several years after the acoustic microscope was invented [2]. The oscillations are quoted as an acoustic materials signature or a $V(z)$ curve [3]. It was clarified [4], [5] that an excitation of a leaky Rayleigh wave plays a central role in the formation of the $V(z)$ curves.

For quantitative measurement of elastic properties, a line-focus-beam (LFB) acoustic microscope was developed [6], and thanks to its superb stability, excitations of many other modes than the leaky Rayleigh wave were identified in the $V(z)$ curves [7]. One of the modes had a phase velocity close to that of a longitudinal wave in the solid, which had been named [8] as a leaky surface skimming compressional wave, or LSSCW in short. But, when we closely examine the measured data, it turns out that the velocity, V_{LSSCW}, is more or less slower than the longitudinal velocity, V_L. It is especially obvious, roughly 100 m/s difference, for hard materials such as hard metals and glasses. For soft materials such as polymers, the difference seems to be small, although unavoidable variation in the velocity and attenuation depending on the production condition of such materials obscures the conclusion.

Chan and Bertoni [9] presented a theory of the LSSCW in the acoustic microscope, extending a ray-optical method originally developed for the leaky Rayleigh wave [10]. They found that the LSSCW can be explained as an excitation of a longitudinal lateral wave, under a condition that a working distance of the acoustical lens, z, is large enough. And the velocity of the lateral wave should be equal to V_L. The condition seems to be satisfied in soft materials, but not in hard materials such as fused quartz [9]. Therefore, theory of the LSSCW for hard materials has not been complete up to now, and it has not been clear whether the difference between V_{LSSCW} and V_L is inherent to the material properties or to the measurement method.

Because a knowledge of the longitudinal velocity is a valuable source of information for the material evaluation of solids [11], it is desired to clarify the physics of the LSSCW in the LFB acoustic microscope. This paper attempts to answer the question by investigating singularities of the acoustical reflection coefficient at a liquid-solid interface and their effect to the $V(z)$ curves.

In the acoustic microscope, an acoustic wave transmitted from a piezoelectric transducer is coupled into a liquid, normally water, through an acoustic lens with a high angle of convergence. The acoustic wave is then reflected by a solid surface and propagated back to the piezoelectric transducer. The convergent acoustic wave can be decomposed into a set of plane waves, called an angular spectrum. The interaction of the plane wave with the solid surface is described by an acoustic reflection coefficient which bears the elastic information of the surface. All the reflected plane wave components integrated on the piezoelectric transducer give rise to a $V(z)$ [12], [13]. Hence, the paper is composed with two major parts, one for the complex analysis of the reflection coefficient with an emphasis on the longitudinal critical angle, and the other for an analysis of $V(z)$ curves especially of the LFB acoustic microscope.

II. Singularities of Reflection Coefficient

A. Branch Point Singularities and Riemann Sheets

The reflection coefficient of an acoustic plane wave incident upon an interface between a liquid and an isotropic solid half

Manuscript received June 7, 1993; revised February 21, 1994; accepted February 23, 1994. The work of Y. Tsukahara was supported by the Summit post-Doctoral Fellowship from Canada. The work of Y. S. Liu was supported by the Natural Science and Engineering Research Council of Canada

Y. Tsukahara was with the Industrial Materials Institute, National Research Council, Boucherville, Québec, Canada J4B 6Y4 on leave from Technical Research Institute, Toppan Printing Co., Ltd., Saitama, Japan 345.

C. Néron and C. K. Jen are with the Industrial Materials Institute, National Research Council, Boucherville, Québec, Canada J4B 6Y4.

Y. Liu is with Department of Electrical Engineering, McGill University, Montreal, Québec, Canada H3A 2A7.

J. Kushibiki is with the Department of Electrical Engineering, Tohoku University, Sendai, Japan 980.

IEEE Log Number 9401977.

space is written as [14]

$$R_{(k_x)} = \frac{(2k_x^2 - k_s^2)^2 + 4k_x^2 k_{lz} k_{sz} - k_s^4 \left(\frac{\rho_w}{\rho_s}\right)\left(\frac{k_{lz}}{k_{wz}}\right)}{(2k_x^2 - k_s^2)^2 + 4k_x^2 k_{lz} k_{sz} + k_s^4 \left(\frac{\rho_w}{\rho_s}\right)\left(\frac{k_{lz}}{k_{wz}}\right)}, \quad (1)$$

where k_x is a wave vector component parallel to the interface, ρ_w and ρ_s are densities of the liquid and solid, respectively, $k_l = \omega/V_L$ and $k_s = \omega/V_s$ are wavenumbers of longitudinal and shear waves in the solid respectively. V_L and V_s are longitudinal and shear wave velocities in the solid, respectively, and ω is the angular frequency. Wave vector components perpendicular to the interface are

$$k_{jz} = \sqrt{k_j^2 - k_x^2}. \qquad (j = l, s \text{ and } w) \quad (2)$$

where $k_w = \omega/V_w$ and V_w is a sound velocity in the liquid. Thus, each k_{jz} has branch points at $k_x = \pm k_j$ in a complex k_x plane, and we take branch cuts emanating from the branch points to keep k_{jz} single valued. Although materials are assumed to be lossless in this paper, they may be lossy in general. Then the wavenumbers become complex, e.g., $k_j \rightarrow k_j + i\alpha$, where α is a positive real number and $i = \sqrt{-1}$. To avoid the real axis from being crossed by the branch cuts in such cases, a cut must be taken from k_j to $k_j + i\infty$, and the other from $-k_j$ to $-k_j - i\infty$. We analyze the branch point singularities of the reflection coefficient at $k_x = k_j$ in the following, but the same argument is also applied to the singularities at $k_x = -k_j$.

When k_x is sufficiently close to k_j, k_{jz} can be approximated by

$$k_{jz} \approx \sqrt{2k_j}\sqrt{k_j - k_x}. \quad (3)$$

Because we choose a principal value for the square root on the real axis of k_x, points 1, 2, 3, and 3′ on the complex k_x plane shown in Fig. 1 are mapped into corresponding points, (1), (2), (3) and (3′) in the complex k_{jz} plane. We call this Riemann sheet of complex k_x a physical plane, because any poles of the reflection coefficient on this plane readily affect its values on the real axis, and k_{jz} satisfies the physical condition for leaky waves [15]. If k_x goes from the point 3 into the clockwise direction, or from the point 3′ into the counter clockwise direction, crossing the branch cut, it is on the other Riemann sheet of k_x, which is called an unphysical plane in this paper. Conventionally, poles on this sheet are discarded because they do not satisfy the physical condition for leaky surface waves [16]. However, these poles sometimes affect the experimental observation [17]–[19], and it is really the case for the LSSCW of the hard materials as shown below.

B. Poles and Zeros of the Reflection Coefficient

Zeros of the numerator and denominator of (1) give zeros and poles, respectively, of the reflection coefficient. We calculated taking water and fused quartz for the liquid and solid, respectively. Material constants used in the calculation are shown in Table I. These values were chosen as representative ones for theoretical calculation. Fig. 2 shows the position of the poles and zeros on the complex k_x plane with numbers from 1 to 7 depicted for their identification. Numerical values of k_x/k_w and a distinction of pole and zero on a particular choice of the Riemann sheets are listed in Table II. On the physical plane, No. 5 and No. 6 are a pole and a zero, respectively, corresponding to the leaky Rayleigh wave [20], [21]. No. 7 close to the water branch point is a pole on the physical plane and known as a Scholte wave which is a special case of a Stonely wave for a liquid/solid interface [22]. Others are all on unphysical planes. No. 3 and No. 4 are very close to the longitudinal branch point, and the particular plane they are on is connected to the physical plane at the longitudinal branch cut. Therefore, their effect cannot be neglected even though they are on the unphysical plane. This is the reason why the phase of the reflection coefficient changes so abruptly at the longitudinal critical angle (thick lines in Fig. 3).

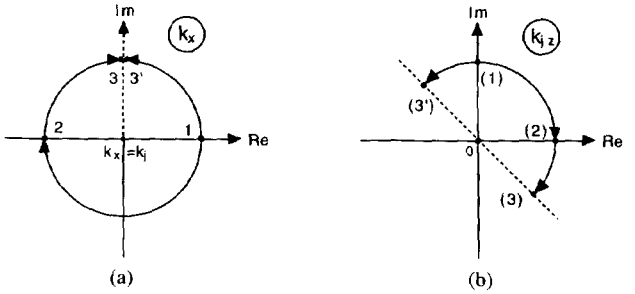

Fig. 1. Complex planes of wave vector components around a branch point. (a) complex k_x plane with a branch cut from $k_x = k_j$ to $k_j + \infty$, (b) complex k_{jz} plane. Points 1, 2, 3 and 3′ on k_x plane correspond to (1), (2), (3), and (3′) on k_{jz} plane.

TABLE I
MATERIAL CONSTANTS USED IN THE CALCULATION OF REFLECTION COEFFICIENT

material	density [kg/m^3]	longitudinal velocity [m/s]	shear velocity [m/s]
fused quartz	2200	5968	3764
gold	19320	3240	1220
water	1000	1500	—
polycarbonate	1190	2300	1000

TABLE II
LOCATION OF POLES AND ZEROS ON RIEMANN SHEETS OF COMPLEX k_x/k_w PLANE OF A REFLECTION COEFFICIENT AT A WATER/FUSED QUARTZ INTERFACE

	Location in Complex k_x/k_w Plane				
		Pole or Zero on Riemann sheet			
No.	k_x/k_w	(ppp)	(upp)	(pup)	(ppu)**
1	0.17200		pole	zero	
2	0.19716		zero	pole	
3	0.25080		zero	pole	
4	0.25106		pole	zero	
5	0.43749+ i 0.01699	pole			zero
6	0.43749- i 0.01699	zero			pole
7	1.00236	pole			zero
* k_x/k_w of branch points		longitudinal 0.25134		shear 0.39851	water 1.00000

**$(a_l a_s a_w)$ is a choice of Riemann sheets for each of longitudinal, shear, and water branch points. p and u for physical and unphysical plane, respectively. Other choices of sheets are equivalent to one of those shown here: $(uuu) = (ppp)$, $(puu) = (upp)$, and $(uup) = (ppu)$.

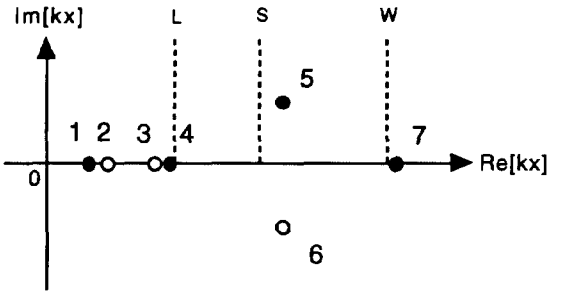

Fig. 2. Location of poles and zeros on the complex k_x plane of a reflection coefficient at an interface between water and fused quartz. Filled and open circles are to show that they are poles and zeros, respectively, on a physical or an adjacent unphysical planes. Numbers are for identification and used also in Fig. 4 and Table II. Dashed lines, depicted with L, $S$and W, are for branch cuts at $k_x = k_l, k_x = k_s$ and $k_x = k_w$, respectively.

The reflection coefficient is conveniently expressed around the longitudinal branch point as

$$R(k_x) = R_0(k_x)\frac{k_{lz} + k_{z0}}{k_{lz} + k_{zp}}. \tag{4}$$

$R_0(k_x)$ is a slowly varying function, and k_{z0} and k_{zp} are introduced by $k_{z0} = \sqrt{k_l^2 - k_0^2}$ and $k_{zp} = \sqrt{k_l^2 - k_p^2}$, respectively, where k_0 and k_p are of the zero and pole (No. 3 and No. 4) close to the branch point, respectively. Because $R(k_x) = 1$ at $k_x = k_l, R_0(k_x) \approx k_{zp}/k_{z0}$ around the longitudinal branch point, and

$$R(k_x) \approx \frac{k_{zp}}{k_{z0}}\frac{k_{lz} + k_{z0}}{k_{lz} + k_{zp}}. \tag{5}$$

The reflection coefficient calculated from (5) is plotted in Fig. 3 with thin lines. The approximation is fairly good.

It should be noted that the approximation in (5) correctly reflects the analytic property of the reflection coefficient around the branch point. On the physical plane it has neither pole nor zero around the branch point, but on the unphysical plane where $k_{lz} \rightarrow -k_{lz}$ it has a pole and a zero at $k_x = k_{zp}$ and $k_x = k_{z0}$, respectively. This explains why the approximation in [9] met the difficulty for the hard materials such as fused quartz.

C. Dependence on Material Constants

If the material constants change, the location of the poles and zeros changes accordingly. For an illustration of this, we change the values of the density, and longitudinal and shear wave velocities simultaneously from those of fused quartz to polycarbonate (a typical polymer). Fig. 4 shows the loci of the poles and zeros, No. 1–No. 4, on the complex k_x plane. They are at positions depicted with their numbers in the figures when the material constants are of fused quartz. They remain on the real axis of the unphysical plane for a while, then rapidly depart from it. When it occurs, the Poison's ratio is 0.33 for poles (No. 1 and No. 4), and 0.23 for zeros (No. 2 and No. 3). It was pointed out [17] that the poles for a solid without liquid loading behave like this at the Poison's ratio equal to 0.264. Thus, soft materials with a large Poison's ratio will not exhibit a very rapid phase change of the

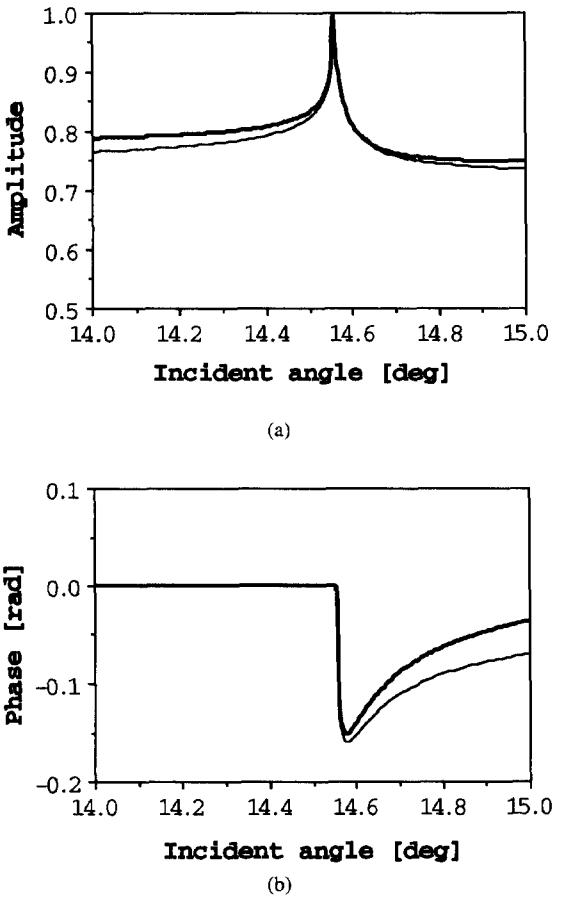

Fig. 3. Incident angular dependence of a reflection coefficient around a longitudinal critical angle of water loaded fused quartz. (a) amplitude, (b) phase. Thick and thin lines are calculated with an exact formula in (1) and an approximation in (5), respectively.

reflection coefficient around the longitudinal critical angle, and the LSSCW analysis of [9] can be applied without difficulty. Finally, the poles and zeros reach to positions depicted with their primed numbers in the figure when the material constants become those of polycarbonate. Dashed lines in the figures indicate the positions of the longitudinal branch cut: one depicted with k_l is for fused quartz and the other with k_l' for polycarbonate. It should be noted that the zero, No. 3, comes out to the physical plane crossing the branch cut, but the other zero and both poles remain on the unphysical plane.

The material constants of the coupling liquid also affect the analytic property of the reflection coefficient. Although most of the acoustic microscopes adopt the distilled water as a coupling liquid, several other materials are used for specific purposes. How the density of the coupling liquid affects the $V(z)$ curve was studied with the experiment and numerical calculation by Doghmane *et al.* [23], and several anomalous features in the $V(z)$ curves were observed when the density became larger. The present scheme might be applied to such problems.

D. Connection to the Pseudo-Sezawa Wave

If we deposit a layer on the solid half space, there appear many other modes guided along the surface [24], and if the shear wave velocity in the layer is slower than that in the

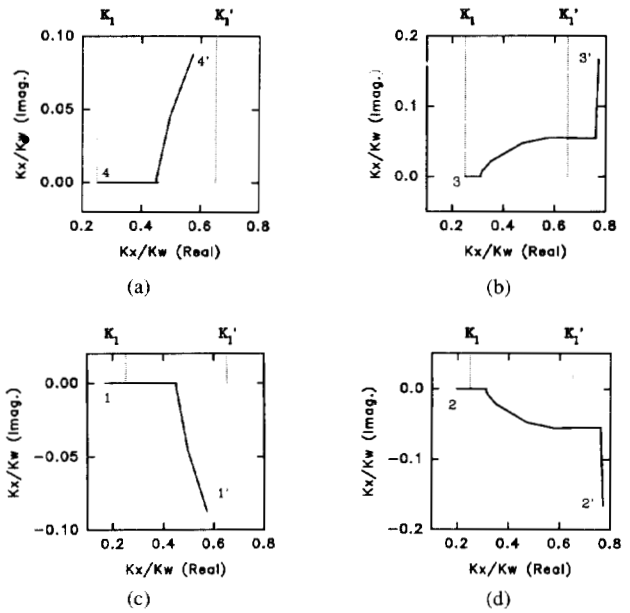

Fig. 4. Loci of poles and zeros on a complex plane k_x as a function of material constants when they are changed from those of fused quartz (number without prime) to polycarbonate (with prime). Numbering of the poles and zeros is also used in Fig. 2 and Table II for identification. Dashed lines with k_l and k_l' are positions of the longitudinal branch cuts for fused quartz and polycarbonate, respectively.

substrate, a Sezawa wave [25] is included in them. With a frequency lower than a cutoff frequency, the Sezawa wave becomes leaky towards the solid substrate, and is called a pseudo-Sezawa wave [26].

A pole and zero associated with the pseudo-Sezawa wave were obtained by a Newton-Raphson's method using a reflection coefficient calculated with a matrix method [27]. A gold layer was assumed on a fused quartz half space. Fig. 5(a) and (b) shows loci of the pole and zero near the shear and longitudinal branch cuts for the substrate as a normalized frequency (fd: f is frequency and d is layer thickness) is varied. When fd becomes smaller the pole and zero get closer to the longitudinal branch point, and in Fig. 5(b) at fd around 4.5 Hzm they submerge into the unphysical plane. At $fd = 0$ Hzm, they reach to the real axis. Therefore, the pole and zero, No. 4 and No. 3, near the longitudinal branch point for the solid half space we discussed above are, in fact, those for the pseudo-Sezawa wave in the limit of $fd = 0$ Hzm.

Fig. 6(a) and (b) shows the amplitude and phase, respectively, of the reflection coefficient of the gold layered fused quartz with different layer thicknesses. It is noticed that the reflection coefficient resembles to that for the layerless case (Fig. 3) when fd is smaller than 10 Hzm. This means that the effects of the pole and branch point are mixed when they are close together regardless whether the pole is on the physical or unphysical plane.

III. $V(z)$ Curves of LFB Acoustic Microscope.

A. Analysis Procedure of V(z) Curves

An elaborate description of $V(z)$ analysis for LFB acoustic microscope is found in [7]. Hence, only a brief summary is presented here.

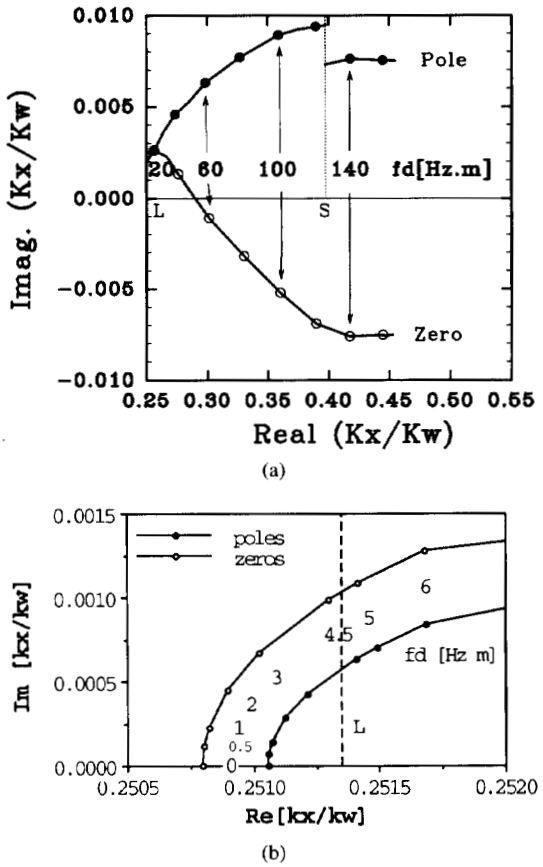

Fig. 5. Loci of pole and zero of a pseudo-Sezawa wave on a complex plane k_x/k_w as a function of normalized frequency, fd. (a) An overall view, and (b) a close up view at the longitudinal branch point of fused quartz substrate. Longitudinal and shear branch points of the substrate, depicted with L and S, are at $k_x/k_w = 0.2513$ and 0.3985, respectively.

In the LFB acoustic microscope, the amplitude $|V|$ is a measurand. The influence of the measurement system, namely the acoustical lens, is eliminated by subtracting a $|V_L(z)|$ curve from a measured $|V(z)|$ curve to give a normalized curve, $V_I(z)$. The $|V_L(z)|$ is obtained by taking a specimen of lead or Teflon which has an almost flat reflection coefficient over the incident angles covered by the acoustical lens. A signal processing, including the digital filtering, is incorporated here to obtain a stable result. $V_I(z)$ then undergoes a spectral analysis to extract an oscillation interval Δz. Fig. 7(a) and (b) shows a $|V(z)|$ and a Fourier transform $F(k)$, respectively, measured of a fused quartz specimen (Toshiba Ceramics Co., T-4040 [28]). Here, the variable k is chosen to be dimensionless, with which Δz is calculated as $\Delta z = \pi/(k_w k)$. To obtain Δz with a sufficient accuracy, care must be taken in choosing an appropriate range and a sampling interval of z to be used in the spectral analysis [7].

B. Theoretical Analysis of $V_I(z)$ Curves

Liang, Kino, and Khuri-Yakub gave a simple expression for $V(z)$ curves [29]. That is, with a slight change of definition,

$$V(u) = \int_0^1 dt L(t) R(t) e^{-iut}. \tag{6}$$

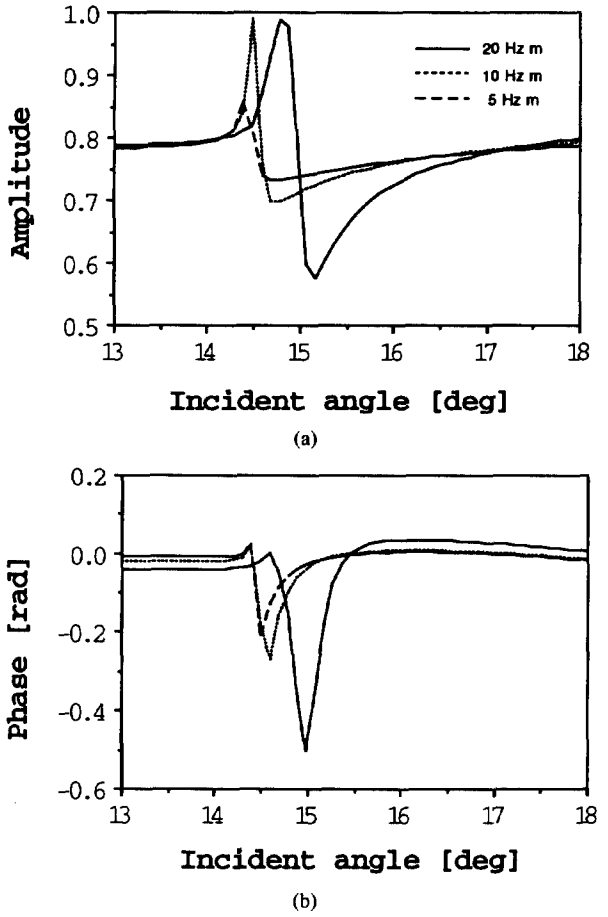

Fig. 6. Incident angular dependence of a reflection coefficient for a gold layered fused quartz loaded with water. (a) Amplitude and (b) phase. $fd = 20$, 10 and 5 Hzm for solid, dotted, and dashed lines, respectively.

We introduced $u = 2zk_w$ and $t = k_{wz}/k_w \equiv \cos\theta$ where θ is an incident angle. $L(t)$ contains a square of a lens pupil function and any other factors due to the system response, and has a feature schematically illustrated in Fig. 8. For a broad range of specimens, we can assume that $R(t)$ is almost constant but has a rapid variation, $R_s(t)$, in several narrow regions of t which correspond to singularities. An example is schematically illustrated in Fig. 8. Then,

$$V(u) \approx \int_0^1 dtL(t)R_0e^{-iut} + \int_0^1 dtL(t)R_s(t)e^{-iut}. \quad (7)$$

The integrand in the first term diminishes more or less smoothly when t decreases to 0, and has a discontinuity at $t = 1$ as shown in Fig. 8. Therefore, the integral can be approximated by

$$\text{The first term} \approx i\frac{R_0L_1}{u}e^{-iu}, \quad (8)$$

where $L_1 \equiv L(t = 1)$. The second term can be modified to

$$\text{The second term} \approx L_s\int_{-\infty}^{+\infty} dtR_s(t)e^{-iut}, \quad (9)$$

where $L_s \equiv L(t = t_s)$, because the integrand has significant values only around $t = t_s$. Thus,

$$V(u) \approx i\frac{R_0L_1}{u}e^{-iu}\left[1 + \frac{uL_s}{iR_0L_1}\int_{-\infty}^{+\infty} dtR_s(t)e^{-iu(t-1)}\right]. \quad (10)$$

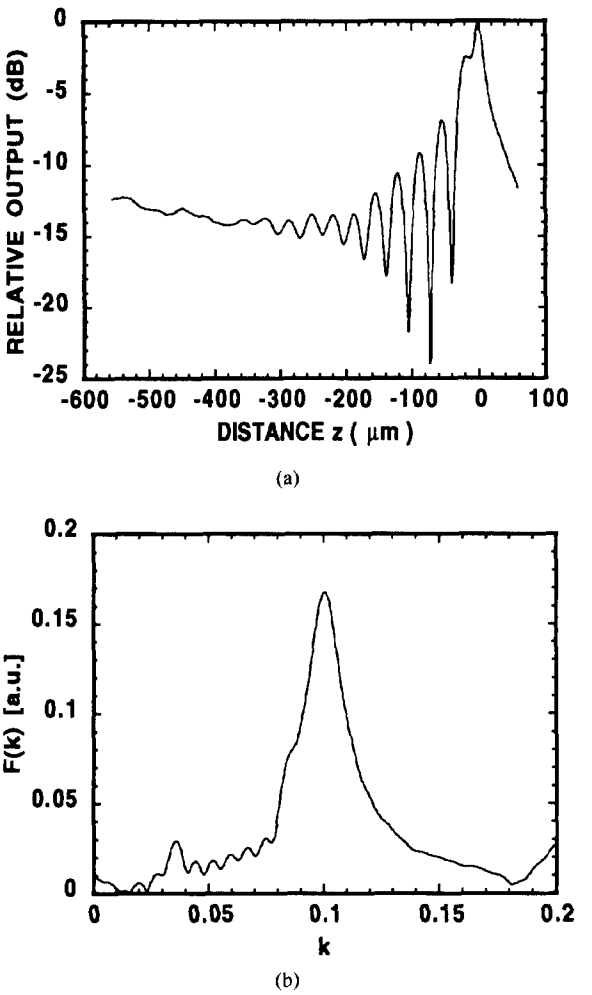

Fig. 7. Experimental $V(z)$ analysis of fused quartz by LFB acoustic microscope. (a) $|V(z)|$ curve, and (b) amplitude of a Fourier transform, $F(k)$. The range of z for FFT is from -40 μm to -454 μm.

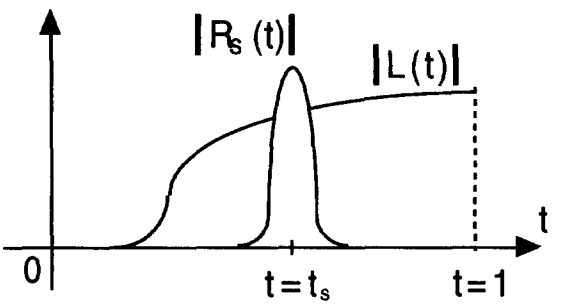

Fig. 8. Schematic illustrations of $L(t)$ and $R_s(t)$. $L(t)$ includes a lens pupil function and other system responses. Examples of actual measurements are found in [29]. $R_s(t)$ is a rapid varying part of a reflection coefficient.

It can be shown [30] that the second term in the square bracket is much smaller than unity in the LFB acoustic microscope, so that the amplitude of $V(u)$ can be expanded as

$$|V(u)| \approx \left|\frac{R_0L_1}{u}\right| \cdot \left\{1 + \frac{1}{2}\left[\frac{uL_s}{iR_0L_1}\int_{-\infty}^{+\infty} dt\ R_s(t)e^{-iu(t-1)} + \text{c.c.}\right]\right\}. \quad (11)$$

where c.c. is for complex conjugate. Because $V_L(u)$ is $V(u)$ with $R_s = 0$,

$$V_I(u) \equiv |V(u)| - |V_L(u)| \approx \frac{L_s}{2i}\left[\int_{-\infty}^{+\infty} dt\ R_s(t)e^{-iu(t-1)} - \text{c.c.}\right]. \quad (12)$$

In the $V(z)$ analysis, we calculate a Fourier spectrum of V_I in a negative region of z. The spectrum is defined as

$$F(k) \equiv \int_{u_0}^{u_1} du e^{iku} V_I(u) \quad (13)$$

where $u_0 < u_1 < 0$. A substitution of (12) into (13) gives an explicit expression,

$$F(k) \approx \frac{L_s \Delta u}{i} e^{i\bar{u}(k+1)} \times \int_{-\infty}^{+\infty} dt\ e^{-i\bar{u}t} R_s(t)\text{sinc}[\Delta u(t-1-k)] - \frac{L_s \Delta u}{i} e^{i\bar{u}(k-1)} \times \int_{-\infty}^{+\infty} dt\ e^{i\bar{u}t} R_s^*(t)\text{sinc}[\Delta u(t-1+k)], \quad (14)$$

where $\bar{u} = (u_1 + u_0)/2$ and $\Delta u = (u_1 - u_0)/2$.$R_s(t)$ differs from zero only when $t \approx t_s$ where $0 < t_s < 1$, and the sinc functions have significant values only when $k \approx t - 1$ and $k \approx 1 - t$ for the first and second term, respectively. Therefore, for positive k, the major contribution comes to the spectrum from the second term, and we obtain,

$$F(k) \approx iL_s \Delta u e^{i\bar{u}(k-1)} \times \int_{-\infty}^{+\infty} dt\ e^{i\bar{u}t} R_s^*(t)\text{sinc}[\Delta u(t-1+k)]. \quad (15)$$

Fig. 9 shows an amplitude of $F(k)$ calculated by (15) for a fused quartz specimen. R_s was calculated by $R_s = R - 1$ where R is an exact formula in (1). $z_0 = -500$ μm and $z_1 = 0$ μm were used. The good agreement with the experimental curve shown in Fig. 7 proves the validity of the theoretical formula. It should be noticed that every singularity in R exhibits itself in $F(k)$ as expected from (15). The Rayleigh wave peak is dominant, and a small peak in the left is of the longitudinal singularity. A slight asymmetry in the Rayleigh wave peak is due to the shear wave singularity which is more clearly seen in the experimental curve in Fig. 7.

C. Estimation of Critical Angles From F(k)

Equation (15) means that the Fourier spectrum of V_I is a convolution of $R_s^*(t)$ and $\text{sinc}[\Delta u(1-t)]\exp\{i\bar{u}(1-t)\}$. If Δu is large enough ($\Delta u \to \infty$), (15) yields a complex conjugate of the reflection coefficient,

$$F(k) \to \frac{iL_s}{\pi} R_s^*(1-k), \quad (16)$$

which contains a full extent of the elastic information of the specimen. However, in reality, the working distance of the lens is limited, so that the sinc function imposes a limitation of the resolution in k as discussed by Liang *et al.* in their inversion of $V(z)$ [29]. The resolution Δt is about

$$\Delta t \approx \frac{\pi}{\Delta u} = \frac{V_w}{2f|z_1 - z_0|}, \quad (17)$$

where f is the frequency. In terms of the incident angle θ, it is

$$\Delta\theta \approx \frac{V_w}{2f|z_1 - z_0|\sin\theta}. \quad (18)$$

Therefore, the estimation of critical angles from $F(k)$ may suffer an error of $\Delta\theta$ in the worst case. For a typical example as in the case of Fig. 7, $f = 225$ MHz, $V_w = 1493$ m/s, $\theta \approx 20°$, and $|z_1 - z_0| = 500$ μm, then the angular resolution $\Delta\theta \approx 1.1°$.

Fortunately, a good approximation of R_s was already derived [20] for the Rayleigh wave,

$$R_s = \frac{k_p^2 - k_0^2}{k_x^2 - k_p^2}. \quad (19)$$

where $k_p = k_R + i\alpha_R$ and $k_0 = k_R - i\alpha_R$. Then the integral in (15) is readily carried out, and the Rayleigh critical angle can be estimated very accurately.

$$F(k) \approx \frac{2L_s \Delta u \alpha}{k_w} e^{i\bar{u}(\cos\theta_R - i\alpha/k_w - 1 + k)} \text{sinc}[\Delta u(\cos\theta_R - i\alpha/k_w - 1 + k)], \quad (20)$$

where $\alpha \equiv \alpha_R \tan\theta_R$ and θ_R is a Rayleigh wave critical angle. In fact, this formula has been used in the LFB acoustic microscope [7] with an acoustic absorption in liquid also taken into account. The relative accuracy of $\pm 0.01\%$ and the absolute accuracy of 0.3% were achieved in the Rayleigh wave velocity measurement [28]. To obtain such an accuracy, care must be taken in the mechanical stability of the apparatus and in the signal processing [7].

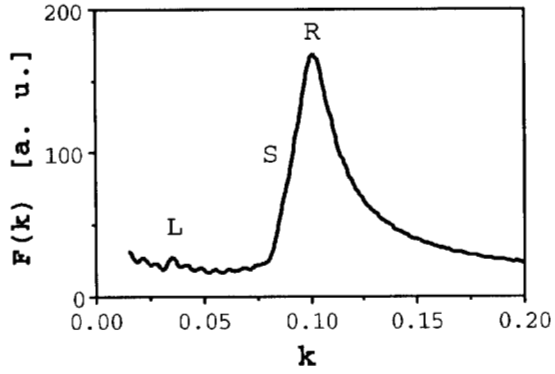

Fig. 9. Amplitude of $F(k)$ theoretically calculated by (15). Exact formula in (1) was used for a reflection coefficient. The range of z is from -50 μm to -550 μm. (R) Rayleigh wave, (S) shear wave, and (L) longitudinal wave critical phenomena.

D. LSSCW

R_s varies gradually, and its variation is symmetric around the Rayleigh critical angle. Thus, the convolution with a sinc function hardly alters the value of the critical angle. This

is another interpretation of the successful estimation of the Rayleigh critical angle. However, this does not hold for the longitudinal critical angle of hard materials as seen in Fig. 3. The reflection coefficient changes abruptly without symmetry because the pole hidden in the unphysical plane is very close to the branch point. And the influence of the dominant Rayleigh wave peak might be another source of difficulty.

In order to eliminate the influence of the Rayleigh wave pole from the LSSCW measurement, a following strategy was implemented into an experiment. A specimen of fused quartz, T-4040 (Toshiba Ceramics Co.), was prepared. The Rayleigh wave velocity and the normalized attenuation factor were measured by using the standard technique [7], $V_R = 3427.0$ m/s and $\alpha = 3.95 \times 10^{-2}$. The parameters were used to synthesize a $V_{RI}(z)$ curve which simulated the $V(z)$ curve due selectively to the Rayleigh wave excitation [Fig. 10(a)]. The $V_{\mathrm{RI}}(z)$ was then subtracted from the measured $V_I(z)$. The remainder, $V_I'(z) = V_I(z) - V_{\mathrm{RI}}(z)$, was subjected to the Fourier analysis to obtain the spectrum, $F(k)$, as shown in Fig. 10(b). There are two major peaks corresponding to the longitudinal and shear critical angles. The longitudinal wave velocity estimated from the left peak was 5899 m/s. A comparison with a bulk wave measurement of 5953 m/s [28] shows that there still remains a difference of 54 m/s (-0.9%). The shear wave velocity estimated from the other peak was 3797 m/s which is 40 m/s ($+1.1\%$) different from a bulk wave measurement of 3757 m/s [28].

During the experiment it was experienced that the estimation of the longitudinal velocity was sensitive to the value of parameters used in the analysis. On the contrary, the shear velocity estimation was rather insensitive to such parameters. For instance, when the starting position z_0 of the window was changed in between 0 and -100 μm, the longitudinal velocity estimation varied roughly ± 100 m/s but the shear velocity estimation remained within ± 25 m/s. This is understood by the fact that the singularity at the shear critical angle is merely a branch point.

Consequently, the method did not remove the effect of the hidden pole in the LSSCW measurement of hard materials such as fused quartz. Therefore, the acoustic microscopist should keep in mind that the LSSCW velocity is slightly slower than the longitudinal wave velocity.

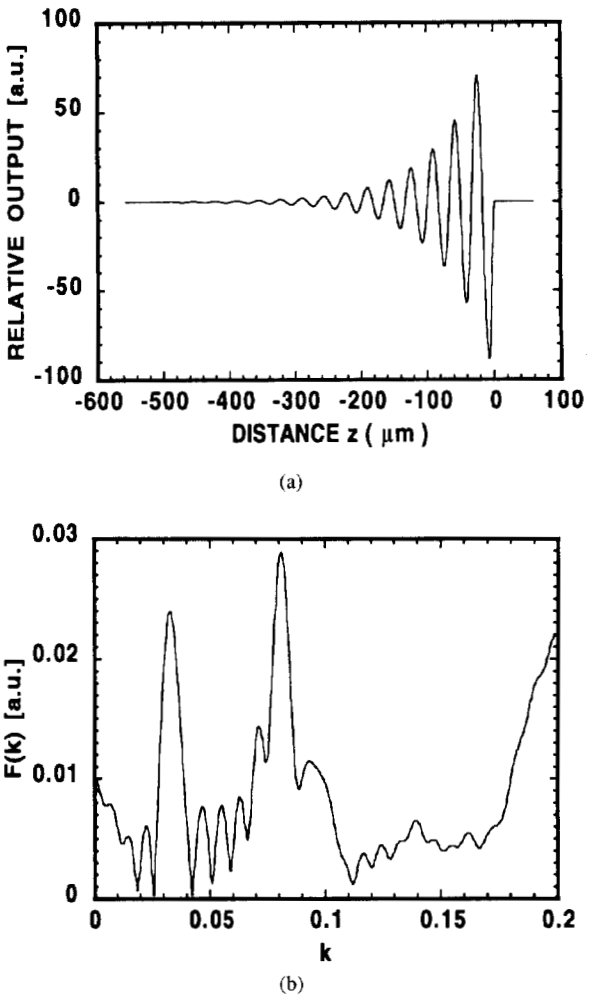

Fig. 10. (a) Synthesized $V_{\mathrm{RI}}(z)$ corresponding to the Rayleigh wave excitation. (b) Amplitude of $F(k)$ calculated from $V_I(z) - V_{\mathrm{RI}}(z)$. Peaks at left and center are of the longitudinal and shear wave critical angles, respectively.

IV. Conclusion

We have shown that a pole hidden on the unphysical Riemann sheet is responsible for the very rapid phase change at the longitudinal critical angle of the reflection coefficient for hard materials. The pole comes out to the physical Riemann sheet as a pseudo-Sezawa wave if a surface layer with a slower material is deposited. For soft materials, the pole is located far from the longitudinal branch point so that it is neglected and the previous approximation [9] might be valid.

It was also shown that the Fourier spectrum $F(k)$ of a normalized $V(z)$ in the LFB acoustic microscope is approximately equal to a varying part of the reflection coefficient, $R_s \approx R - 1$, convolved with a sinc function which represents a finite working distance of the lens movement. Therefore, the reflection coefficient might be recovered, in principle, if a suitable technique of deconvolution is applied to $F(k)$. This is left for a future study.

For isotropic materials, the Rayleigh wave singularity is dominant, and variation of the reflection coefficient is smooth and symmetric around the Rayleigh critical angle. Hence, the Rayleigh wave velocity and attenuation can be very accurately estimated as demonstrated in [7], [28]. However, at the longitudinal critical angle, the variation is abrupt and not symmetric because of the presence of the hidden pole. Then, the convolution with a sinc function causes a shift of the peak in the Fourier spectrum $F(k)$. The dominant Rayleigh wave pole also induces the shift. These are cause of the velocity difference between the LSSCW and the longitudinal wave.

It was demonstrated that, by suitably subtracting a synthesized $V(z)$ curve corresponding to the Rayleigh wave excitation, the influence of the Rayleigh wave pole can be removed from the LSSCW measurement. In addition, we have identified and measured the shear critical angle in $F(k)$ for the fused quartz sample. After removing the Rayleigh wave influence, it was found that the estimation of the shear velocity is rather stable than that of the longitudinal velocity. This

suggests that the shear velocity estimation could be useful for the elastic characterization of hard materials.

However, this does not necessarily means the technique can be applied to all materials. If, for example, the specimen is anisotropic or with a layered structure, then singularities of the reflection coefficient have a more complicated analytic structure than that of an isotropic half space. Therefore, to interpret the $V(z)$ measurement, it is important to study the analytic structure of the reflection coefficient.

The LSSCW measurement of soft materials such as polymers is hardly affected by the hidden pole. However, it is subject to the influence of bulk wave attenuation. Therefore, to fully utilize the LSSCW measurement for soft materials, which is of engineering importance, the velocity and attenuation must be carefully calibrated by the LSSCW and bulk wave measurements. This must be undertaken in the future study.

ACKNOWLEDGMENT

Authors are grateful to Dr. J. D. Dai of IMI, NRC, for helping in the calculation with Mathematica and to Dr. M. Viens of IMI, NRC for discussions on singularities on complex Riemann sheets. Y. Tsukahara acknowledges Toppan Printing Co., Ltd. which generously permitted one year leave.

REFERENCES

[1] R. D. Weglein and R. G. Wilson, "Characteristic material signatures by acoustic microscopy," *Electron. Lett.*, vol. 14, pp. 352–354, 1978.
[2] R. A. Lemons and C. F. Quate, "A scanning acoustic microscope," in *Proc. 1973 IEEE Ultrason. Symp.*, pp. 18–20, 1973.
[3] A. Atalar, C. F. Quate, and H. K. Wickramasinghe, "Phase imaging in reflection with the acoustic microscope," *Appl. Phys. Lett.*, vol. 31, pp. 791–793, 1978.
[4] W. Parmon and H. L. Bertoni, "Ray interpretation of the material signature in the acoustic microscope," *Electron. Lett.*, vol. 15, pp. 684–686, 1979.
[5] A. Atalar, "A physical model for acoustic signatures," *J. Appl. Phys.*, vol. 50, pp. 8237–8239, 1979.
[6] J. Kushibiki, A. Ohkubo and N. Chubachi, "Linearly focused acoustic beams for acoustic microscopy," *Electron. Lett.*, vol. 17, pp. 520–522, 1981.
[7] J. Kushibiki and N. Chubachi, "Material characterization by line-focus-beam acoustic microscope," *IEEE Trans. Sonics Ultrason.*, vol. SU-32, pp. 189–212, 1985.
[8] R. D. Weglein, "A model for predicting acoustic material signatures," *Appl. Phys. Lett.*, vol. 34, pp. 179–181, 1979.
[9] K. H. Chan and H. L. Bertoni, "Ray representation of longitudinal lateral waves in acoustic microscopy," *IEEE Trans. Ultrason., Ferroelec., Freq. Contr.* vol. 38, pp. 27–34, 1991.
[10] H. L. Bertoni, "Ray-optical evaluation of $V(z)$ in the reflection acoustic microscope," *IEEE Trans. Sonics Ultrason.*, vol. SU-31, pp. 105–116, 1984.
[11] C. K. Jen, Z. Wang, A. Nicolle, C. Neron, E. L. Adler, and J. Kushibiki, "Acoustic graded-index lenses," *Appl. Phys. Lett.*, vol. 59, pp. 1398–1400, 1991.
[12] A. Atalar, "An angular spectrum approach to contrast in reflection acoustic microscopy," *J. Appl. Phys.*, vol. 49, pp. 5130–5139, 1978.
[13] H. K. Wickramasinghe, "Contrast in reflection acoustic microscopy," *Electron. Lett.*, vol. 14, pp. 305–306, 1978.
[14] See for instance L. M. Brekhovskikh and O. A. Godin, *Acoustics of Layered Media I.* Berlin: Springer-Verlag, 1990.
[15] G. W. Farnell, "Properties of elastic surface waves," in *Physical Acoustics VI*, W. P. Mason and R. N. Thurston, Eds. New York: Academic, 1970, pp. 109–166.
[16] L. M. Brekhovskikh, *Waves in Layered Media.* New York: Academic, 1980, pp. 49–50.
[17] J. A. Hudson, *The Excitation and propagation of Elastic Waves.* London: Cambridge Univ., 1980, pp. 169–172.
[18] F. Gilbert and S. J. Laster, "Excitation and propagation of pulses on an interface," *Bull. Seismol. Soc. Amer.*, vol. 52, pp. 299–319, 1962.
[19] E. Strick, "Propagation of elastic wave motion from an impulsive source along a fluid/solid interface," *Phil. Trans. Roy. Soc. London, A*, vol. 251, pp. 465–523, 1959.
[20] H. L. Bertoni and T. Tamir, "Unified theory of Rayleigh angle phenomena for acoustic beams at liquid-solid interfaces," *J. Appl. Phys.*, vol. 2, pp. 157–172, 1973.
[21] L. M. Brekhovskikh, *Waves in Layered Media.* New York: Academic, 1980, pp. 41–50.
[22] H. Uberall, "Surface waves in acoustics," in *Physical Acoustics X*, W. P. Mason and R. N. Thurston, Eds. New York: Academic, 1973, pp. 1–10.
[23] A. Doghmane, Z. Hadjoub, K. Alami, J-M. Saurel, and J. Attal, "Effects of couplant mass loading on the acoustic signature $V(z)$," *J. Acoust. Soc. Amer.*, vol. 92, pp. 1545–1550, 1992.
[24] B. A. Auld, *Acoustic Fields and Waves in Solids Vol. II,* New York: Wiley, 1973, pp. 94–104.
[25] K. Sezawa and K. Kanai, "Discontinuity in the dispersion curves of Rayleigh waves," *Bull. Earthquake Res. Inst.*, vol. 13, pp. 238–244, 1935.
[26] Y. Tsukahara, E. Takeuchi, E. Hayashi and Y. Tani, "A new method of measuring surface layer-thickness using dips in angular dependence of reflection coefficients," *Proc. IEEE 1984 Ultrason. Symp.*, pp. 992–996.
[27] L. M. Brekhovskikh, *Waves in Layered Media.* New York: Academic, 1980, pp. 53–60.
[28] J. Kushibiki, T. Wakahara, T. Kobayashi and N. Chubachi, "A calibration method of the LFB acoustic microscope system using isotropic standard specimens," *Proc. IEEE 1992 Ultrason. Symp.*, pp. 719–722.
[29] K. K. Lian, G. S. Kino, and B. T. Khuri-Yakub, "Material characterization by the inversion of $V(z)$," *IEEE Trans. Sonics Ultrason.*, vol. SU-32, pp. 213–224, 1985.
[30] A. Briggs, *Acoustic Microscopy.* Oxford: Oxford Univer., 1992, pp. 130–144.

Yusuke Tsukahara (M'84) was born in Chiba Prefecture, Japan, on June 25, 1952. He received the B.S. degree in physics from Waseda University, Tokyo, Japan, in 1976 and the Ph.D. degree in electrical engineering from Tohoku University, Sendai, Japan, in 1990.

From 1976 to 1982 he was engaged in research and development of instruments for nondestructive testing at Ishikawajima Inspection Services Co. Ltd, Tokyo, Japan. Since 1982, he has been with Technical Research Institute of Toppan Printing Co. Ltd., Saitama, Japan, where he is currently an assistant chief researcher. He has been involved in the study of surface layers by ultrasonic spectroscopy since 1984. In 1986 he stayed at Tohoku University, Sendai, Japan, as a visiting researcher. His current interests include speech analysis, laser generation of ultrasound, ultrasonic microspectrometer and its application to the material characterization.

Dr. Tsukahara is a member of Acoustical Society of Japan. He received the Outstanding Paper Award of the 1989 IEEE TRANSACTIONS ON ULTRASONICS, FERROELECTRICS, AND FREQUENCY CONTROL, and the Best Paper Award of the 1988 Bulletin of the Japanese Society of Printings and Technology.

Yongshen Liu was born in Fujian, China, on March 17, 1963. He received the B.Eng. and M.Eng. degrees, both in electronic engineering, in 1984 and 1986, respectively, from the Tsinghua University, Beijing, China.

Currently, he is working toward the Ph.D. degree with the Department of Electrical Engineering, McGill University, Montreal, PQ, Canada. His recent research involves material characterization using acoustic microscopy.

Christian Néron received the D.E.C. in 1978 from Cegep La Pocatiere, Canada.

Since 1980 he has been engaged in ultrasonic research at the Industrial Materials Institute, NRC, as a technical officer. He is currently involoved with ultrasonic characterization methods including microscopy and imaging.

C. K. Jen (M'84–SM'88), photograph and biography not available at the time of publication.

Jun-ichi Kushibiki (M'83), photograph and biography not available at the time of publication.